-synuclein insertion into supported lipid bilayers as seen by in situ x-ray reflectivity

Hähl, Hendrik ; Möller, Isabelle ; Kiesel, Irena ; Campioni, Silvia ; Riek, Roland ; Verdes, Dorinel ; Seeger, Stefan

Abstract: Large aggregates of misfolded -synuclein inside neuronal cells are the hallmarks of Parkinson's disease. The protein's natural function and its supposed toxicity, however, are believed to be closely related to its interaction with cell and vesicle membranes. Upon this interaction, the protein folds into an -helical structure and intercalates into the membrane. In this study, we focus on the changes in the lipid bilayer caused by this intrusion. In situ X-ray reflectivity was applied to determine the vertical density structure of the bilayer before and after exposure to -synuclein. It was found that the -synuclein insertion, wild type and E57K variant, caused a reduction in bilayer thickness. This effect may be one factor in the membrane pore formation ability of -synuclein.

DOI: https://doi.org/10.1021/cn5002683

Originally published at:
Hähl, Hendrik; Möller, Isabelle; Kiesel, Irena; Campioni, Silvia; Riek, Roland; Verdes, Dorinel; Seeger, Stefan (2015). -synuclein insertion into supported lipid bilayers as seen by in situ x-ray reflectivity. ACS Chemical Neuroscience, 6(3):374-379.
DOI: https://doi.org/10.1021/cn5002683

α-Synuclein Insertion into Supported Lipid Bilayers As Seen by in Situ X-ray Reflectivity

Hendrik Hähl,[†,§] Isabelle Möller,[†] Irena Kiesel,[‡,∥] Silvia Campioni,[¶] Roland Riek,[¶] Dorinel Verdes,[†] and Stefan Seeger[*,†]

Department of Chemistry, University of Zurich, Winterthurerstrasse 190, 8057 Zurich, Switzerland, Fakultät Physik/DELTA Technische Universität Dortmund, 44221 Dortmund, Germany, and Laboratory of Physical Chemistry, Department of Chemistry and Applied Biosciences, Swiss Federal Institute of Technology Zurich, Wolfgang-Pauli-Str. 10, 8093 Zurich, Switzerland

E-mail: sseeger@chem.uzh.ch

Abstract

Large aggregates of misfolded α-synuclein inside neuronal cells are the hallmarks of Parkinson's disease. The protein's natural function and its supposed toxicity, however, are believed to be closely related to its interaction with cell and vesicle membranes. Upon this interaction, the protein folds into an α-helical structure and intercalates into the membrane. In this study, we focus on the changes in the lipid bilayer caused by this intrusion. In situ X-ray reflectivity was applied to determine the vertical density structure of the bilayer before and after exposure to α-synuclein. It was found that the α-synuclein insertion, wild type and E57K variant, caused a reduction in bilayer thickness. This effect may be one factor in the membrane pore formation ability of α-synuclein.

[*]To whom correspondence should be addressed

[†]Uni Zurich

[‡]TU Dortmund

[¶]ETH Zurich

[§]Current address: Department of Experimental Physics, Saarland University, D-66123, Saarbrücken, Germany

[∥]Current address: Institut Laue-Langevin, 71 avenue des Martyrs, 38000 Grenoble, France

Keywords

α-synuclein, Parkinson's disease, supported lipid bilayer, X-ray reflectivity

Introduction

Neurodegenerative age-related diseases like Parkinson's disease are increasingly common. Parkinson's disease is pathologically marked by the development of Lewy bodies, i. e. proteinaceous inclusion bodies in intracerebral neurons (*1*). These inclusion bodies are enriched in distinct proteins, with their major component being α-synuclein (*2*). Therefore α-synuclein is believed to be involved in the pathogenesis of this disease. This hypothesis is supported by the fact that several point mutations of α-synuclein lead to a severe and early onset form of the disease (*3*). Nevertheless, the role of α-synuclein in the pathogenesis of the disease as well as its normal function in healthy cells is still under discussion: It is suspected, that α-synuclein plays a role in transmitter release, although it is not clear whether promoting or inhibiting (*4*, *5*). Additionally, it is believed to be involved in the whole process of synaptic vesicle recycling (*6*).

α-Synuclein is a protein consisting of 140

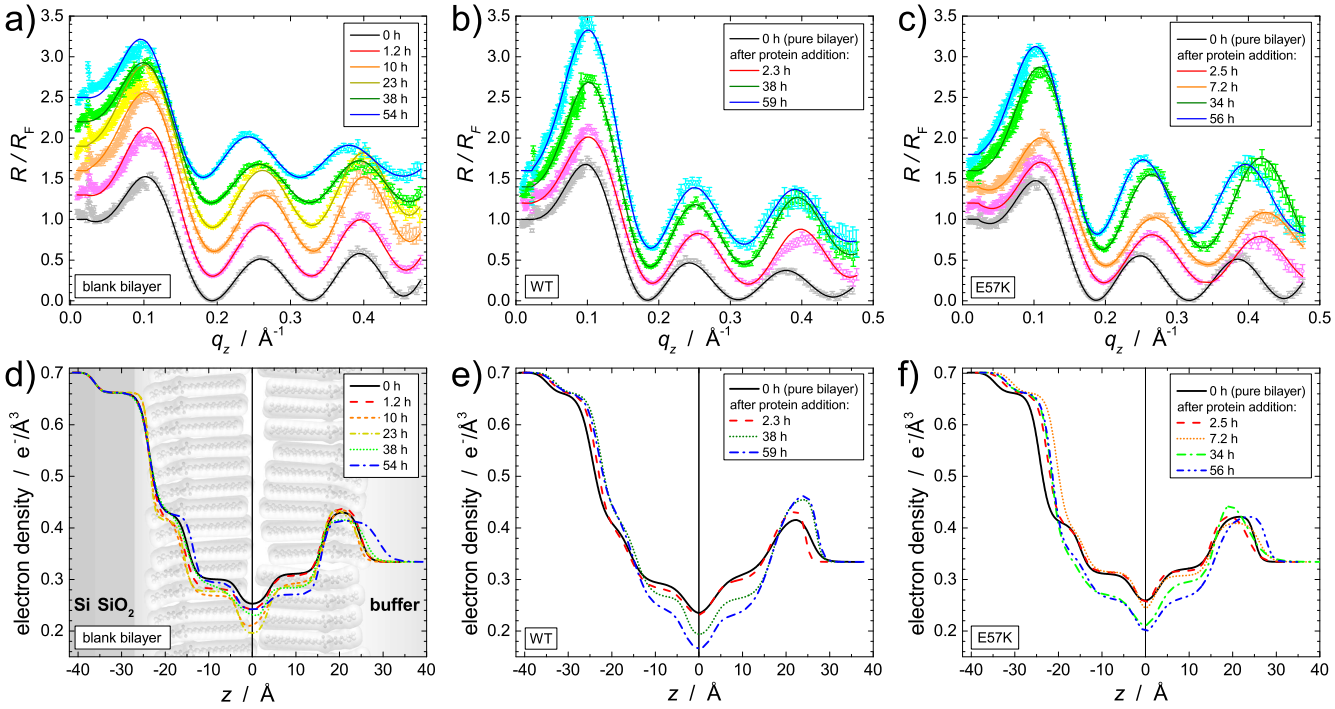

Figure 1: (a)–(c): Recorded reflectivity data normalized to the Fresnel reflectivity R_F of an ideal flat silicon substrate: (a) blank bilayer, (b) with wild type α-synuclein, and (c) with E57K variant. Subsequent measurements are shifted along the ordinate for better readability. (d)-(f) EDPs as received from the refinement procedure of the respective data presented above. The profiles were shifted along the abscissa to align the bilayer center. In the background of (d) the layer system used for data modeling is illustrated.

amino acids with a molecular weight of 14.5 kDa, is unstructured in solution, and folds into α-helices upon interaction with membranes (*7*). A misfolding of the protein into a β-sheet structure leads to aggregation into oligomers, protofibrils, and eventually to mature filaments. The transition states between monomer and filament are believed to be the toxic species involved in Parkinson's disease. Although it is still not clear what exactly causes the toxicity, it seems to be intimately related to the interaction of α-synuclein with the cell membrane. Upon this interaction the protein may cause a disruption or permeabilization of the cell membrane, which then leads to a neuron loss (*8–11*).

To further elucidate the interactions of α-synuclein with lipid membranes, we aim at measuring the changes of the bilayer upon incorporation of α-synuclein and its development thereafter. In addition to the wild type form of α-synuclein we also utilized its strongly toxic mutant E57K (*12*). The structure of the membrane before and after α-synuclein incorporation was probed via X-ray reflectometry (XRR). With this technique, it is possible to probe the vertical density structure of stratified samples with angstrom resolution. Using high beam energies as available at synchrotron light sources allows for a penetration of the beam through water and hence also enables in situ characterization of solid liquid interfaces. XRR could recently be successfully applied in several in situ studies of biological interfaces as protein films (*13*, *14*) and lipid bilayers (*15*, *16*). Here, it allows us to monitor the changes of lipid membranes due to the interaction with α-synuclein.

Results and Discussion

Reflectivity experiments were performed with wild type (WT) α-synuclein as well as with the

mutant E57K. Moreover as a reference, the development of a blank bilayer without protein addition was recorded. The measured data are presented in Figure 1 a–c. The solid lines represent the calculated reflectivities obtained from the model refinement. The model electron density profiles (EDPs) corresponding to these reflectivities are presented in panels d–f below the respective data. To highlight changes in the bilayer structure, EDPs are aligned at the bilayer center.

The obtained profiles display clearly the features of a lipid bilayer: regions of higher electron density symmetrically at distances of ca. 15–24 Å from the bilayer center, representing the lipid head groups including phosphate group, functional group, water molecules, and counterions. From ca. 3 to 15 Å, regions with electron densities lower than the one of the surrounding buffer represent the hydrocarbon tails of the lipid. At the bilayer center, a region of even more decreased electron density exists, where the electron poor CH_3 end groups come into contact (cf. Figure 1 d). The thickness of the whole bilayer directly after the preparation varies slightly for each experiment with a mean value of 49.3(9) Å. Thereby the thickness is measured as the distance between the inflection points in the profiles representing the upper/lower boundary of the upper/lower headgroup. Overall, the obtained profiles agree well with results from simulations (*23*) and from similar experiments (*24*, *25*). The errors for the individual electron density and thickness values determined as descried above were typically about 1% and 2%, respectively, and thus smaller than the differences between separate experiments. The magnitude of the errors compares well with results from other XRR studies of biological samples (*13*, *14*, *25*).

The most obvious change in the EDPs over time for all experiments is the decrease in the electron density in the tail group region of the bilayer, i. e. about ±15 Å around the bilayer center. To quantify this decrease, the integral of the EDPs over the tail group region was calculated. As boundaries for these integrals, the inflection points in the EDPs, which represent the interface between lipid head groups and tail

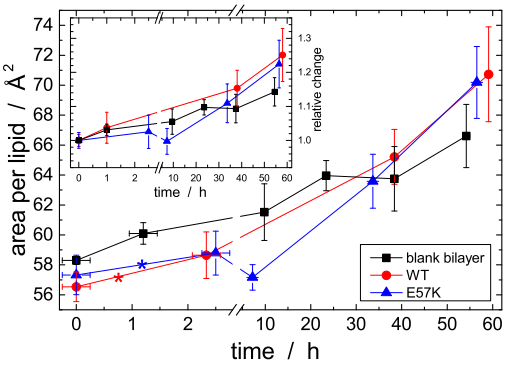

Figure 2: Area per lipid as calculated from the number of electrons in the tail group regions of the EDPs. Time is set to zero for the first measurement. The errors along the time axis indicate the length of one measurement (ca. 30 min). The asterisks mark the time of the protein injection. The inset shows the data normalized to their initial value.

groups, were chosen. The result of this calculation is the number of electrons per area in the tail group region. Comparing these values with the theoretical number of electrons of one lipid tail group, i. e. 270, the average area per lipid can be calculated. These values are presented in Figure 2. The overall trend for all experiments is the same: The area per lipid increases continuously without much difference between the individual experiments. It should be noted that this method of calculating the lipid density assumes that only lipid tails contribute to the measured electron density. Especially a potential intrusion of parts of the protein is neglected. The small differences between the values of separate experiments and their course over time, however, justifies this assumption and moreover shows that there is no or only a nondetectable intrusion of the protein between the lipid tail groups.

After injecting the protein, a clear effect of the protein on the bilayer can be observed: Already in the reflectivity data, a wavelength shift in the oscillations indicates a reduction of the film thickness. Extracting the thickness of the bilayer from the EDPs, this reduction can be quantified (see Figure 3): About 1 h after the protein injection, the bilayer thickness de-

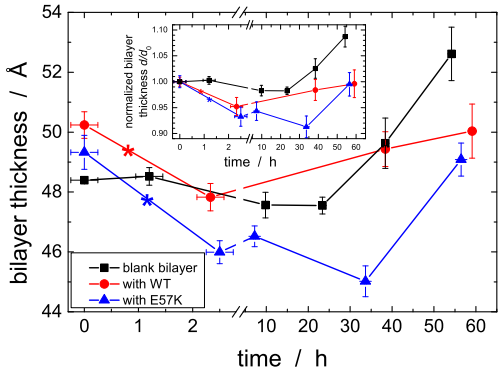

Figure 3: Development of the bilayer thickness with time. Errors in time and asterisks have the same meaning as in Figure 2. The inset shows the data normalized to their initial value. A clear reduction in thickness can be seen after protein injection.

creases around 5% and 7% for the WT and the E57K, respectively. Interestingly, the thickness of both bilayer leaflets decreases. Such a thickness reduction does not occur for the blank bilayer. More than 2 days after the bilayer preparation, all bilayers tended to increase in thickness again, yet a clear difference between the bilayers with protein and the blank bilayer remained. Particularly, the thickness of bilayers with incorporated α-synuclein did not exceed its initial value in the course of the experiments. A reduction of the bilayer's thickness was also inferred by Pfefferkorn et al. (*24*) and Hellstrand et al. (*28*) from neutron reflectometry measurements, yet with a smaller value for the reduction as well as a considerable higher uncertainty.

The effect of α-synuclein on the thickness of the lipid bilayer may be explained by the following model: As the thickness reduction is found for both leaflets of the bilayer, the most plausible explanation for this observation is a flattening or smoothing of the bilayer: Assuming the protein does not extract lipids upon its insertion (since there is no density reduction purely associated with the insertion process), there has to be an increase in lipid density locally around the protein. This higher density should induce better packing and hence better lateral ordering of the lipid tails, which would also be accompanied by better vertical ordering. Additionally, the space beneath the protein may be filled by hydrocarbon chains from the neighboring lipids undergoing gauche–trans conformations or by lipids from the lower leaflet interdigitating into the upper leaflet (cf. Figure 4). These effects were also recently proposed by Ouberai et al. (*30*). Yet, the notion that the decreased thickness is merely an average value and might be much bigger at the protein sites (as e. g. proposed by Pfefferkorn et al. (*24*)) is not supported by our data as this would translate into an EDP smeared out at the interface between lipid heads and tails. Instead, the data and the obtained EDPs rather hint at a decreased interfacial roughness after protein insertion. Thus, a small but spacious thickness reduction or just a smoothing of the bilayer is a better interpretation of the results. An increase in lipid packing density around the inserted protein, however, is yet a hypothesis remaining to be tested with different methods. Nonetheless, it might explain the ability of α-synuclein to affect the membrane curvature: In the case of unsupported bilayers or vesicles, the lipids could restore their former density by an increase in curvature (*30*). In our experiment, the attractive forces to the substrate (*31*) may inhibit this behavior.

The thickness decrease of the bilayer could also play a role in the pore formation process and bilayer leakage reported after α-synuclein insertion (*9*, *32*). At and around the protein insertion site, particularly if lower leaflet lipids interdigitate, a penetration of the bilayer may be facilitated especially upon oligomerization. The E57K variant is known to be more prone to oligomerization and thus more toxic than the wild type α-synuclein (*12*). In the experiments presented here, a slightly higher value for the bilayer thickness reduction than caused by the wild type is found. Different effects could lead to this observation: A true larger reduction in bilayer thickness where the protein is inserted caused by deeper interdigitation of lipids from the lower leaflet, a larger ordered and smoothed area around the protein, or a larger adsorbed amount of protein. Although it cannot be decided which of these effects or even a combination applies here, all of them may enhance

the probability of pore formation and hence the higher toxicity of the E57K variant may at least be partly explained.

As the effect of α-synuclein on the bilayer is clearly visible, the question arises, where the protein is situated. From Figure 2, it is clear that there is no detectable portion of the protein in the lipid tail group region. Yet, an intrusion of α-synuclein into the bilayer is highly expected at least in the upper headgroup region (*24*, *26–28*). Inspecting these regions in the EDPs (see Figure 1 e,f), it is obvious that their electron density does not decrease as it is the case for the tail groups but stays constant or even increases in the case of the WT data. However, calculating the number of electrons per area in the headgroup regions, no clear difference between blank bilayer and bilayer with protein can be determined with our data. The reason for this might be the small amount of inserted protein: The pure, unhydrated protein has an electron density of ca. $0.57\,\mathrm{e}^-/\mathrm{\AA}^3$ (as calculated from the protein database entry 1XQ8 (*29*)), which is well above the headgroup's electron density (determined here on average as $0.428(5)\,\mathrm{e}^-/\mathrm{\AA}^3$). Thus, one should expect an increase in the electron density and the number of electrons in the headgroup region upon protein insertion, especially if the lipid density does not change much, which is the case for the first measurement after protein insertion. In recent studies, however, the amount of adsorbed (or inserted) α-synuclein to lipid bilayers similar to the one used in this study was determined. It was found that the ratio of protein to lipid mass was around 0.025 (*26*, *30*). From this value, an expected change in the electron density can be calculated as around 0.8%. As this change is smaller than the error in the electron density, it becomes obvious that it is not possible to detect this change unmistakably in the headgroup region. However, an intrusion into the lipid tail groups or an adsorption on top of the bilayer should be visible due to the higher contrast but cannot be inferred from the presented reflectivities: A replacement of lipid tails by proteins or protein parts would increase the electron density by more than 1% already for a protein fraction of only 1.2%. Similar values are obtained for the region above the head groups. Moreover, the assumption of another layer on top of the lipids did not lead to better fits of the data but rather unphysical EDPs. Thus, the data show that the main part of α-synuclein indeed inserts into the headgroup region of the lipids. This is well in line with findings that the α-helical parts of α-synuclein are well embedded in the lipid headgroup (*26*, *27*). From recent neutron reflectometry studies, an additional layer on top of the bilayer was proposed (*24*, *28*). In accordance with QCM-D measurements, this layer has a low density and a thickness of up to 8 nm (*28*) and is supposed to represent the C-termini of α-synuclein tangling in the solution (*26*). This is not in contradiction with our data since the contrast in electron density of such a layer to the surrounding water phase may not be large enough to be detectable in our measurements.

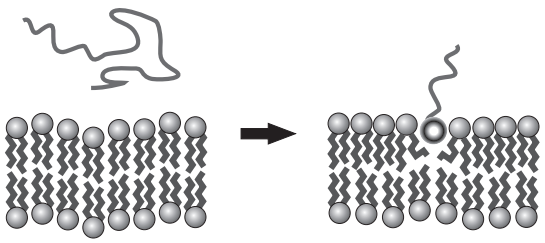

Figure 4: Model for the change in bilayer structure after α-synuclein insertion: The protein inserts deeply into the lipid head groups and thereby increases the local lipid density and hence the ordering of the lipids. Below the protein, a void is created that may be filled by neighboring lipid tails and/or interdigitating lipids from the lower leaflet. In sum, the average thickness of the bilayer is reduced.

Additionally to what has been discussed, what is not seen in the data is also noteworthy: Even after 2 days, the bilayers seem to be stable as no signs for destruction of the bilayer due to α-synuclein insertion are visible in the data: Although a decrease in lipid density is observed, this decrease is not clearly different from the density decrease of the blank bilayer. Thus, a thinning out of the bilayer due to α-synuclein insertion cannot be supported by the data for the given experimental condi-

tions. Moreover, large holes in the bilayer with diameters in the micrometer range can also be excluded. Such a scenario would yield reflectivities composed as linear superposition of signals from bilayer covered and clear substrate sites as e. g. reported by Wang et al. (*16*). Yet, it is not possible to explain the recorded data with a superposition model. Partial or complete bilayer destruction, however, was reported in other studies with similar bilayer composition and similar or even lower α-synuclein concentrations (*10*, *33*). There may be several reasons why we do not observe membrane destruction in the presented experiments: First of all, the bilayer's lipid density as determined from the data is quite high in the beginning. This may lead to a lower incorporation of α-synuclein molecules. Since the lipid density is, however, not always given or determined in many other studies, it is hardly possible to compare. Moreover, we used a silicon wafer as support for the bilayer, which provides higher attractive forces than the common microscope slide (*14*, *31*) and hence may further stabilize the bilayer. Yet, most likely the reason lies with the protein itself: It is widely believed that membrane instability, pore formation, and fibrillation at the membrane are started by small α-synuclein oligomers or protofibrils (*9*). Using a thorough purification protocol for the protein, we ensured that practically only monomers were used in the measurements. Nevertheless, the notion exists that the interaction with the membrane and the locally increased concentration of α-synuclein might facilitate dimerization and thus start the oligomerization (*8*, *11*). In our experiments, the protein concentration in the bilayer might be too low even to start this process. Pores, however, might be present. Yet, if no larger membrane destruction occurs and the pores are not as numerous as to decrease the average density of the bilayer measurably, these pores will not be visible with reflectivity methods. Summarizing, this means that with respect to the data we can definitely exclude a bilayer destruction; pores in the bilayer may exist, yet.

Conclusion

In this study, XRR was applied to monitor the changes in the structure of supported lipid bilayers upon exposure to α-synuclein. It was found that α-synuclein inserts into the lipid headgroup region of the bilayer. This insertion leads to a decrease in the average thickness of the bilayer whereas the overall lipid density is not affected. This may be interpreted as a flattening or smoothing of the bilayer. A change in stability of the bilayer due to protein insertion, however, was not observed.

Materials and Methods

α-Synuclein Samples The proteins (wild type α-synuclein and the E57K variant) were expressed, purified, and prepared as samples for the experiments as described previously (*17*). The purity of the proteins was at least 98%. They were prepared dissolved in PBS (Sigma-Aldrich) with 0.05% NaN_3 with a concentration determined individually for each sample via UV–vis absorbance measurements at $\lambda = 280\,\mathrm{nm}$. The protein solutions were stored at 4 ℃ until usage. The volume of the protein solution used for the experiments was adjusted to yield a final protein concentration in the measurement cell of 10 µM.

Substrate Preparation As support for the lipid bilayers, pieces from a silicon wafer (Si-Mat Silicon Materials, Kaufering, Germany) with a native silicon oxide layer were used. The pieces (ca. $1.5 \times 1.5\,\mathrm{cm}^2$) were cleaned in piranha solution (1:1 mixture of H_2O_2 and H_2SO_4) and rinsed afterward several times in boiling Milli-Q water. Until use, these substrates were stored in Milli-Q water. For the bilayer preparation as well as for the reflectivity experiments, the substrates were put into a metallic sample cell. The cell was a hollow cube covered with gold on the inner side with two facing windows covered with kapton foil. A sample holder also covered with gold fixed the substrate inside the cell. Thus, the only materials in contact with the added fluid were gold,

silicon, and the kapton of the cell windows.

Supported Lipid Bilayers Supported lipid bilayers were prepared following a modified protocol of Richter et al. (*18*). In short, 1,2-dioleoyl-*sn*-glycero-3-phospho-L-serin (DOPS) and 1,2-dioleoyl-*sn*-glycero-3-phosphocholine (DOPC) (Avanti Polar Lipids) in chloroform were used as received and mixed at a ratio of 35:65. The lipid was dried overnight under vacuum to remove the solvent and then resuspended in Tris buffer (149 mM NaCl, 5 mM $CaCl_2$, 10 mM Tris) to a final concentration of 0.1 g/L. The resulting solution was extruded 29 times through a membrane (pore size 0.1 µm) to produce unilamellar vesicles. The vesicle solution was put directly in the measurement cell containing the silicon substrate. There the solution was left more than 1 h, whereafter it was replaced by the pure Tris buffer. Subsequently, this solution was exchanged again by a Ca^{2+} free Tris buffer (10 mM Tris, 133 mM NaCl) containing 5 mM EDTA in order to remove the Ca^{2+} ions, and finally by PBS. All buffers contained 0.05% NaN_3 and were adjusted to pH 7.4. A reflectivity measurement directly after the completion of this protocol yielding a clear bilayer signature ensured the successful buildup of the bilayer.

X-ray Reflectivity (XRR) XRR experiments were performed at the beamline BL9 of the DELTA synchrotron radiation facility in Dortmund, Germany (*19*). For the measurements, a photon energy of 27 keV was chosen balancing between flux and transmission through water while reducing simultaneously the possible beam damage (*15*). The specular reflectivity was determined as a function of the incident angle θ. The diffuse background was recorded after each scan using an offset of 0.1° to the specular angle. Reflectivities could be recorded up to $\theta = 1°$ with satisfying statistics. Each sample was measured before and after protein injection and again in nonuniform time intervals of several hours. Every measurement was repeated at least once to ensure a steady state for the duration of the measurement and in order to exclude possible changes due to beam damage. All experiments were performed at room temperature.

Data Analysis The obtained reflectivity data were background and footprint corrected. They are presented here as a function of the scattering vector

$$q_z = \frac{4\pi}{\lambda} \sin\theta \ .$$

Moreover, the data are normalized to the Fresnel reflectivity R_F, i. e. the theoretical reflectivity of the bare, ideal flat silicon substrate. Thus, the strong decrease in the reflectivity ($\propto q_z^4$), which ranges here over 7 orders of magnitude, is removed, and the oscillations that are indicative for surface films are highlighted.

To obtain structural information, the electron density profile (EDP) of the sample is modeled and its theoretical reflectivity is calculated. The model can then be refined in order to fit its reflectivity to the data. The applied model was generated employing the "effective density" approach (*20*), which ensures continuous EDPs even in the case of high interfacial roughness values compared to the respective layer thickness. It consists of six layers accounting for "SiO_2 layer / lower lipid headgroup / lower lipid tail group / depletion layer / upper lipid tail group / upper lipid headgroup" (cf. Figure 1d). The parameters describing this model (layer thickness, interfacial roughness, and electron density for each layer) were then again refined using a least-squared fitting routine (LSfit) to obtain the reflectivity best resembling the experimental data. In this routine, the EDP is cut into roughness free slices of less than 0.1 Å thickness, on which then the Parratt algorithm (*21*) is applied. Electron densities of Si and SiO_2 were fixed to their literature values (0.698 and 0.646 $e^-/Å^3$) (*22*). Their interface roughness and the SiO_2 film thickness were not varied after once determined in the reference measurement. The errors for the obtained parameter values were estimated as the changes in each parameter that were necessary to increase the mean square variation χ^2 of the respective best fit by at least 5%.

Author Information

Author Contribution H.H., S.S., and D.V. designed the study. S.C. and R.R. produced and purified the proteins. H.H. and I.M. developed experimental methods and performed the experiments with help from I.K. H.H. and I.K. analyzed the data. H.H., D.V., S.S., and I.M. discussed the results. H.H. wrote the paper with contributions from I.M., S.C., I.K., D.V., and S.S.

Funding This work was supported by the Swiss National Science Foundation (SNSF), the German Federal Ministry of Education and Research (BMBF) (Project 05K10PEC) and the Cluster of Excellence RESOLV (EXC1069) funded by the German Research Foundation (DFG).

Notes The authors declare no competing financial interest.

Acknowledgement The authors thank Dr. Christian Sternemann (TU Dortmund) for help in performing the experiments and fruitful discussions as well as Jonas Heppe, Mischa Klos, Christian Kreis, and Christian Spengler (all Saarland University, Saarbrücken, Germany) for assistance during the experiments. The DELTA machine group is gratefully acknowledged for providing synchrotron radiation and technical support.

References

1. Braak, H., Ghebremedhin, E., Rüb, U., Bratzke, H., and Tredici, K. D. (2004) Stages in the development of Parkinson's disease-related pathology. *Cell Tissue Res 318*, 121–34.

2. Spillantini, M. G., Schmidt, M. L., Lee, V. M., Trojanowski, J. Q., Jakes, R., and Goedert, M. (1997) Alpha-synuclein in Lewy bodies. *Nature 388*, 839–40.

3. Zarranz, J. J., Alegre, J., Gómez-Esteban, J. C., Lezcano, E., Ros, R., Ampuero, I., Vidal, L., Hoenicka, J., Rodriguez, O., Atarés, B., Llorens, V., Tortosa, E. G., del Ser, T., Muñoz, D. G., and de Yebenes, J. G. (2004) The new mutation, E46K, of alpha-synuclein causes Parkinson and Lewy body dementia. *Ann Neurol 55*, 164–73.

4. Cabin, D. E., Shimazu, K., Murphy, D., Cole, N. B., Gottschalk, W., McIlwain, K. L., Orrison, B., Chen, A., Ellis, C. E., Paylor, R., Lu, B., and Nussbaum, R. L. (2002) Synaptic vesicle depletion correlates with attenuated synaptic responses to prolonged repetitive stimulation in mice lacking alpha-synuclein. *J Neurosci 22*, 8797–807.

5. Abeliovich, A., Schmitz, Y., Fariñas, I., Choi-Lundberg, D., Ho, W. H., Castillo, P. E., Shinsky, N., Verdugo, J. M., Armanini, M., Ryan, A., Hynes, M., Phillips, H., Sulzer, D., and Rosenthal, A. (2000) Mice lacking alpha-synuclein display functional deficits in the nigrostriatal dopamine system. *Neuron 25*, 239–52.

6. Cheng, F., Vivacqua, G., and Yu, S. (2011) The role of α-synuclein in neurotransmission and synaptic plasticity. *J Chem Neuroanat 42*, 242–8.

7. Davidson, W. S., Jonas, A., Clayton, D. F., and George, J. M. (1998) Stabilization of alpha-synuclein secondary structure upon binding to synthetic membranes. *J Biol Chem 273*, 9443–9.

8. Auluck, P. K., Caraveo, G., and Lindquist, S. (2010) α-Synuclein: membrane interactions and toxicity in Parkinson's disease. *Annu Rev Cell Dev Biol 26*, 211–33.

9. van Rooijen, B. D., Claessens, M. M. A. E., and Subramaniam, V. (2010) Membrane Permeabilization by Oligomeric α-Synuclein: In Search of the Mechanism. *PLoS ONE 5*, e14292.

10. Reynolds, N. P., Soragni, A., Rabe, M., Verdes, D., Liverani, E., Handschin, S.,

Riek, R., and Seeger, S. (2011) Mechanism of Membrane Interaction and Disruption by alpha-Synuclein. *J Am Chem Soc 133*, 19366–19375.

11. Rabe, M., Soragni, A., Reynolds, N. P., Verdes, D., Liverani, E., Riek, R., and Seeger, S. (2013) On-surface aggregation of α-synuclein at nanomolar concentrations results in two distinct growth mechanisms. *ACS Chem Neurosci 4*, 408–17.

12. Winner, B. et al. (2011) In vivo demonstration that alpha-synuclein oligomers are toxic. *P Natl Acad Sci USA 108*, 4194–9.

13. Richter, A. G., and Kuzmenko, I. (2013) Using in situ X-ray reflectivity to study protein adsorption on hydrophilic and hydrophobic surfaces: benefits and limitations. *Langmuir 29*, 5167–80.

14. Hähl, H., Evers, F., Grandthyll, S., Paulus, M., Sternemann, C., Loskill, P., Lessel, M., Hüsecken, A. K., Brenner, T., Tolan, M., and Jacobs, K. (2012) Subsurface Influence on the Structure of Protein Adsorbates as Revealed by in Situ X-ray Reflectivity. *Langmuir 28*, 7747–7756.

15. Reich, C., Hochrein, M., Krause, B., and Nickel, B. (2005) A microfluidic setup for studies of solid-liquid interfaces using X-ray reflectivity and fluorescence microscopy. *Rev Sci Instrum 76*, 095103.

16. Wang, S. T., Fukuto, M., and Yang, L. (2008) In situ x-ray reflectivity studies on the formation of substrate-supported phospholipid bilayers and monolayers. *Phys Rev E 77*, 31909.

17. Campioni, S., Carret, G., Jordens, S., Nicoud, L., Mezzenga, R., and Riek, J. (2014) The presence of an air-water interface affects formation and elongation of α-synuclein fibrils. *J Am Chem Soc 136*, 2866–75.

18. Richter, R., Mukhopadhyay, A., and Brisson, A. (2003) Pathways of lipid vesicle deposition on solid surfaces: a combined QCM-D and AFM study. *Biophys J 85*, 3035–47.

19. Paulus, M., Lietz, D., Sternemann, C., Shokuie, K., Evers, F., Tolan, M., Czeslik, C., and Winter, R. (2008) An access to buried interfaces: The X-ray reflectivity set-up of BL9 at DELTA. *J Synchrotron Rad 15*, 600–605.

20. Tolan, M. *X-ray scattering from soft-matter thin films*; Springer tracts in modern physics 148; Springer: Heidelberg, 1999.

21. Parratt, L. G. (1954) Surface studies of solids by total reflection of X-rays. *Phys Rev 95*, 359–369.

22. The Center for X-ray Optics. `http://www.cxro.lbl.gov/`.

23. Böckmann, R. A., Hac, A., Heimburg, T., and Grubmüller, H. (2003) Effect of sodium chloride on a lipid bilayer. *Biophys J 85*, 1647–55.

24. Pfefferkorn, C. M., Heinrich, F., Sodt, A. J., Maltsev, A. S., Pastor, R. W., and Lee, J. C. (2012) Depth of α-synuclein in a bilayer determined by fluorescence, neutron reflectometry, and computation. *Biophys J 102*, 613–21.

25. Reich, C., Horton, M. R., Krause, B., Gast, A. P., Rädler, J. O., and Nickel, B. (2008) Asymmetric structural features in single supported lipid bilayers containing cholesterol and GM1 resolved with synchrotron X-Ray reflectivity. *Biophys J 95*, 657–68.

26. Wietek, J., Haralampiev, I., Amoussouvi, A., Herrmann, A., and Stöckl, M. (2013) Membrane bound α-synuclein is fully embedded in the lipid bilayer while segments with higher flexibility remain. *Febs Lett 587*, 2572–7.

27. Perlmutter, J. D., Braun, A. R., and Sachs, J. N. (2009) Curvature dynamics of alpha-synuclein familial Parkinson disease mutants: molecular simulations of the

micelle- and bilayer-bound forms. *J Biol Chem 284*, 7177–89.

28. Hellstrand, E., Grey, M., Ainalem, M.-L., Ankner, J., Forsyth, V. T., Fragneto, G., Haertlein, M., Dauvergne, M.-T., Nilsson, H., Brundin, P., Linse, S., Nylander, T., and Sparr, E. (2013) Adsorption of α-Synuclein to Supported Lipid Bilayers: Positioning and Role of Electrostatics. *ACS Chem Neurosci 4*, 1339–1351.

29. Ulmer, T. S., Bax, A., Cole, N. B., and Nussbaum, R. L. (2005) Structure and dynamics of micelle-bound human alpha-synuclein. *J Biol Chem 280*, 9595–603.

30. Ouberai, M. M., Wang, J., Swann, M. J., Galvagnion, C., Guilliams, T., Dobson, C. M., and Welland, M. E. (2013) α-Synuclein senses lipid packing defects and induces lateral expansion of lipids leading to membrane remodeling. *J Biol Chem 288*, 20883–95.

31. Loskill, P., Hähl, H., Faidt, T., Grandthyll, S., Müller, F., and Jacobs, K. (2012) Is adhesion superficial? Silicon wafers as a model system to study van der Waals interactions. *Adv Colloid Interfac 179-182*, 107–13.

32. Zakharov, S. D., Hulleman, J. D., Dutseva, E. A., Antonenko, Y. N., Rochet, J.-C., and Cramer, W. A. (2007) Helical alpha-synuclein forms highly conductive ion channels. *Biochemistry 46*, 14369–79.

33. Zhu, M., Li, J., and Fink, A. L. (2003) The association of alpha-synuclein with membranes affects bilayer structure, stability, and fibril formation. *J Biol Chem 278*, 40186–97.

Graphical TOC Entry

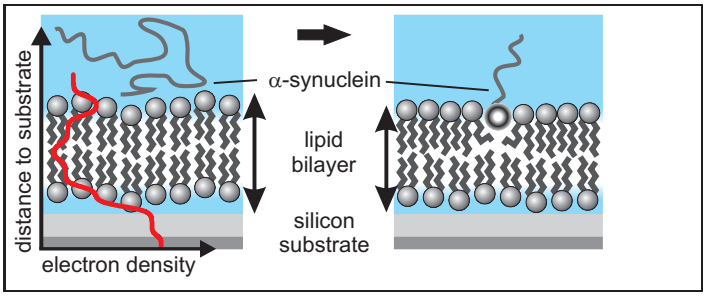

α-Synuclein Insertion into Supported Lipid Bilayers as seen by in situ X-Ray Reflectivity

Hendrik Hähl, Isabelle Möller, Irena Kiesel, Silvia Campioni, Roland Riek, Dorinel Verdes, and Stefan Seeger.